Supplemental Methods

Sex as a biological variable

Our study examined male and female animals, and similar findings are reported for both sexes (Supplemental Tables 2 and 3).

Animals

Wild-type C57BL/6J mice were purchased from The Jackson Laboratory (Bar Harbor, ME) and used for behavioral, electrophysiological, morphological, and molecular experiments. *Aldh1l1*-Cre/ERT2 × ROSA26-Lck-GCaMP6f-flox mice were used for astrocytic Ca^{2+} imaging studies. Mice were 6–8 weeks old at the start of experimental procedures and were housed under a 12-h light/dark cycle with food and water available ad libitum.

Viral vectors

For astrocytic D1R knockdown, recombinant adeno-associated viral vectors (AAVs) were used to express a microRNA-adapted short hairpin RNA (shRNAmir) targeting the mouse dopamine D1 receptor gene (*Drd1*). The shRNA target sequences (bwD1a: 5′-ACCGATGTCTCTCTAGAAA-3′) and (bwD1b: 5’-CCACTTTGTATTTATGTAA-3’) were embedded in two concatenated miR-30 backbones with a bulge in the stem, cloned into the 3’UTR of the viral vector plasmid (1), and expressed under the control of the astrocyte-selective GfaABC1D promoter. AAVs included AAV2/5-GfaABC1D-shD1R-GFP, AAV2/5-GfaABC1D-shD1R-tdTomato, AAV2/5-GfaABC1D-GFP, and AAV2/5-GfaABC1D-tdTomato (titer $\geqslant 4.1 \times 10^{12}$ viral genomes/ml). All

viruses were packaged as serotype 5 by the University of North Carolina Gene Therapy Center Vector Core.

Primary astrocyte cultures

Primary astrocyte cultures were prepared from the striatum of postnatal day 0 (P0) or P1 mice. Dissection and dissociation were performed as previously described (2). A total of 10^6 cells per well in a poly-D-lysine-coated 6-well plate were plated into 5% Serum Medium, MEM with Earle's salts (Millipore Sigma M4655), supplemented with 5% fetal bovine serum and 0.2% MITO+ Serum-Extender (Corning, #355006). Cells were transduced at 7 days in vitro (DIV) with 4 µl AAV and harvested on DIV28.

Semiquantitative RT-PCR

Primary astrocytes transduced with AAVs were washed with PBS with Ca^{2+} and Mg^{2+} and lysed in Trizol (Thermo-Fisher). RNA was isolated following the manufacturer's protocol. Using random primers, cDNA synthesis was performed as described previously (2). PCRs were performed for mouse *Drd1* with the intron flanking primers (5'-GAGTCCAGGGGTTTTGGGAG -3') and (5'-GGCTTAGCCCTCACGTTCTT-3'), and for GAPDH with the intron flanking primers (5'-TCAGGAGAGTGTTTCCTCGTC-3') and (5'-GATGGGCTTCCCGTTGATGA-3').

Single-nucleus RNA sequencing

Bilateral NAcSh tissues were collected from cocaine- or saline-trained mice (n = 5 per group), snap-frozen on dry ice, and stored at −80 °C until use. Single-nucleus isolation was performed

following the 10x Genomics protocol (CG000124, Isolation of Nuclei for Single Cell RNA Sequencing), as previously described (3). snRNA-seq libraries were prepared using the GEM-X Universal 3′ Gene Expression v4 kit (10x Genomics). Isolated nuclei and barcoded gel beads, together with reverse transcription reagents, were loaded into the Chromium X system to generate single-nucleus gel bead-in-emulsions (GEMs). Following cDNA amplification and cleanup, libraries were constructed through cDNA fragmentation, end repair and A-tailing, adaptor ligation, and sample index PCR. Library concentrations were quantified using a Qubit 4.0 fluorometer (Life Technologies), and library quality was assessed using a TapeStation 2200 (Agilent Technologies). Pooled libraries were sequenced on an Illumina NextSeq 2000 using paired-end sequencing (Read 1: 28 bp; i7 index: 10 bp; i5 index: 10 bp; Read 2: 90 bp), with an average sequencing depth of ~30,000 reads per nucleus.

Single-nucleus RNA-seq data analysis

Raw sequencing data were processed using Cell Ranger (v9.0.0; 10x Genomics) for sample demultiplexing, barcode processing, UMI counting, and alignment to the mouse reference transcriptome (GRCm39-2024-A). The resulting UMI count matrices were imported into Seurat (v5.3.0) (4) in R (v4.5.1) for downstream analysis. Nuclei were excluded if they contained fewer than 300 detected genes, fell within the top 2% of total UMI counts, or contained more than 15% mitochondrial gene content. Doublets were identified and removed using scDblFinder (v1.22.0) (5). After quality control and filtering, 11,029 nuclei from saline-treated mice and 17,611 nuclei from cocaine-treated mice were retained for analysis. Gene expression data were log-normalized using the Seurat function NormalizeData and scaled using ScaleData. The top 2,000 highly variable genes were identified using FindVariableFeatures with the “vst” method and used to compute the first 30 principal components. Clustering was performed using the Seurat function

FindClusters. Differential gene expression between conditions was assessed using FindMarkers with the MAST test (test.use = "MAST"), requiring a minimum expression in 20% of nuclei (min.pct = 0.2), an adjusted p value < 0.05, and a log fold-change threshold of 0.38.

In vivo virus injection

Mice were anesthetized by intraperitoneal injection of a ketamine (100 mg/kg)–xylazine (10 mg/kg) mixture and placed in a stereotaxic frame (Stoelting Co., Wood Dale, IL). Using a 10-μL NanoFil syringe fitted with a 32-gauge needle and controlled by a UMP3 Micro4 pump system (World Precision Instruments, Sarasota, FL), AAV solutions were bilaterally infused into the NAcSh at a rate of 200 nL/min (500 nL per hemisphere; coordinates relative to bregma: AP +1.60 mm, ML ±0.70 mm, DV −4.45 mm). The needle was left in place for an additional 5 min after infusion to allow diffusion and minimize backflow.

Catheter implantation

Catheter implantation for cocaine self-administration was performed as previously described (6-8). Briefly, a silastic catheter was advanced approximately 1 cm into the right jugular vein, and the distal end was tunneled subcutaneously to exit at the back between the scapulae. Catheters were constructed from silastic tubing (length, 7 cm; inner diameter, 0.30 mm; outer diameter, 0.64 mm) and connected to a Vascular Access Button (Instech). Mice were allowed to recover for at least 3 days following surgery, during which general health and body weight were monitored. During the recovery period, catheters were flushed daily with sterile saline containing cefazolin (3 mg/mL) and heparin (3 U/mL) to prevent infection and maintain catheter patency.

Self-administration apparatus

All behavioral experiments were conducted in operant conditioning chambers (Med Associates). Each chamber (15.24 × 13.34 × 12.7 cm) was equipped with one active and one inactive lever, a conditioned stimulus (CS) light positioned above the active lever, and a house light. No food or water was available in the chamber during training or testing sessions.

Intravenous cocaine self-administration

Cocaine self-administration training began at least 3 days after surgery. During the 5-day training period, mice were placed in the operant chamber for daily 6-hour sessions. Presses on the active lever resulted in an infusion of cocaine (1 mg/kg delivered over 3-6 s) and simultaneous illumination of the CS light above the lever and the house light. Both the CS light and house light remained illuminated for 20 s, during which additional lever presses were recorded but did not result in further cocaine infusions. Presses on the inactive lever had no reinforced consequences but were recorded. After the 5-day training period, mice were returned to their home cages and remained there during the abstinence period. Cocaine-trained mice that failed to meet the self-administration criteria ($\geqslant$60 infusions per session and $\geqslant$70% of total lever presses on the active lever) were excluded from further experimentation and analysis. For electrophysiological recordings on abstinence day 1, mice were used 1 day after the final training session. For recordings on abstinence day 45, mice were singly housed in their home cages throughout the 44-day abstinence period, with food and water available ad libitum.

Cocaine extinction and cue-induced reinstatement of cocaine seeking

The extinction procedure consisted of 2-h daily sessions conducted for 10 consecutive days. During each session, mice were placed in the same operant chambers used for cocaine self-administration; active lever presses did not result in cocaine infusion or presentation of CS cues. Cue-induced reinstatement tests consisted of 2-h daily sessions for 3 consecutive days in the same chambers, in which active lever presses presented the cocaine-paired light cue without cocaine infusion. In both procedures, inactive lever presses were recorded but had no programmed consequences. One shD1R mouse was removed for health reasons after the completion of self-administration training and was therefore included in the training analysis (n = 7) but not in the extinction and reinstatement analyses (n = 6).

Preparation of acute brain slices

Mice were decapitated under deep isoflurane anesthesia. Coronal brain slices (250 μm thick) containing the nucleus accumbens (NAc) were prepared using a VT1200S vibratome (Leica) in ice-cold cutting solution containing (in mM): 135 N-methyl-D-glucamine, 1 KCl, 1.2 KH_2PO_4, 0.5 $CaCl_2$, 1.5 $MgCl_2$, 20 choline bicarbonate, and 11 glucose. The solution was saturated with 95% O_2 / 5% CO_2, adjusted to pH 7.4 with HCl, and osmolality was adjusted to 305 mmol kg^{-1}. Slices were then transferred to artificial cerebrospinal fluid (aCSF) containing (in mM): 119 NaCl, 2.5 KCl, 2.5 $CaCl_2$, 1.3 $MgCl_2$, 1 NaH_2PO_4, 26.2 $NaHCO_3$, and 11 glucose, with osmolality adjusted to 285–295 mmol kg^{-1}. Slices were incubated in oxygenated aCSF (95% O_2 / 5% CO_2) at ~34°C for 30 min and subsequently maintained at 20–22°C for at least 30 min before experimentation.

Electrophysiological recordings

Whole-cell patch-clamp recordings were performed to examine membrane properties of astrocytes and synaptic transmission onto NAcSh MSNs. All recordings were obtained from the ventromedial NAcSh.

For synaptic transmission recordings, MSNs closely adjacent to astrocytic GFP fluorescence were preferentially selected. During recordings, slices were superfused with aCSF preheated to 30–32°C using a feedback-controlled in-line heater (Warner). To measure minimal stimulation–evoked responses and NMDAR-mediated EPSCs, recording electrodes (2–5 MΩ) were filled with a Cs^+-based internal solution containing (in mM): 135 $CsMeSO_3$, 5 CsCl, 5 TEA-Cl, 0.4 EGTA (Cs), 20 HEPES, 2.5 Mg-ATP, 0.25 Na-GTP, and 1 QX-314 (Br), pH adjusted to 7.3. Picrotoxin (0.1 mM) was included in the aCSF during all recordings to inhibit $GABA_A$ receptor-mediated currents. Presynaptic afferents were stimulated using a constant-current isolated stimulator (Digitimer) through a monopolar electrode (glass pipette filled with aCSF). Series resistance was typically 7–20 MΩ, left uncompensated but monitored continuously. Cells exhibiting changes in series resistance >20% were excluded from analysis. Synaptic currents were recorded using a MultiClamp 700B amplifier, filtered at 2.6–3 kHz, amplified fivefold, and digitized at 20 kHz.

To record NMDAR-mediated EPSCs, the AMPAR-selective antagonist NBQX (5 μM) was added to the bath solution. The membrane potential was held at −40 mV to relieve Mg^{2+}-dependent block of NMDARs. Stimulation position and intensity were then held constant. Following a 10-min baseline recording, a bath solution containing the GluN2B-selective antagonist Ro256981 (200 nM) was perfused into the recording chamber. Given the wash-in time and use-dependent nature of Ro256981, EPSCs recorded 10 min after antagonist application were used to assess Ro256981-sensitive NMDAR currents. After 20-min of recording in Ro256981 bath, a bath

containing APV (50 μM) instead of Ro256981 was applied to confirm that the recorded EPSCs were NMDAR-mediated.

Silent synapses were assessed using the minimal stimulation assay as previously described (9-12). Briefly, after obtaining small (~50 pA) EPSCs at −70 mV, stimulation intensity was gradually reduced until synaptic failures and successes could be clearly distinguished. Stimulation intensity and frequency were then held constant for the remainder of the experiment. The minimal stimulation assay was performed in the absence (vehicle) or presence of the CP-AMPAR–selective antagonist Naspm (1-naphthyl acetyl spermine trihydrochloride, 200 μM; Tocris, #2766), which was bath-applied and allowed to equilibrate for 10 min before the assay. For each neuron, 50–100 traces were recorded at −70 mV and +50 mV, and recordings were repeated for one to two additional rounds. Only neurons exhibiting stable failure rates (changes <15% between rounds) were included in the analysis. Failures and successes were visually scored in a blinded manner to minimize bias.

The percentage of silent synapses was calculated based on two assumptions: (1) presynaptic release sites are independent, and (2) release probability is identical across all synapses, including silent synapses. Under these assumptions, silent synapse percentage was calculated as:

$$silent\ synapse\ (\%) = 1 - \frac{ln(F_{-70})}{ln(F_{+50})}$$

where F_{-70} and F_{+50} represent failure rates at −70 mV and +50 mV, respectively (12). It is worth noting that cocaine experience increases presynaptic release probability within several glutamatergic projections to NAcSh MSNs (13), but this does not affect the assessment of silent synapses using the above equation, because in the same mouse the release probability was cancelled out during assessment. Furthermore, it remains undetermined whether the release probability at silent versus non-silent synapses differ in cocaine-trained animals, mainly due to

technical difficulties recording a single synapse. Even it is different, this equation could still be used to qualitatively predict changes in silent synapse levels, as previously validated (14).

Paired-pulse ratio (PPR) was assessed in MSNs adjacent to GFP^+ astrocytes. MSNs were voltage-clamped at −70 mV, and two consecutive stimuli were delivered to presynaptic afferents at an interstimulus interval of 50 ms, with the stimulation intensity adjusted to evoke a first EPSC of approximately 100 pA. Paired stimuli were delivered every 20 s. PPR was calculated from the averaged trace as the amplitude of the second EPSC divided by that of the first (EPSC2/EPSC1), with both amplitudes measured from the pre-stimulus baseline.

To assess electrophysiological properties of astrocytes, whole-cell recordings were obtained from NAcSh astrocytes identified by GFP expression driven by AAV2/5-GfaABC1D-GFP. Recording electrodes (4–6 MΩ) were filled with a K^+-based internal solution containing (in mM): 135 K-gluconate, 5 KCl, 0.4 EGTA, 10 HEPES, 2.5 Mg-ATP, and 0.3 Na-GTP (pH 7.3, adjusted with KOH), supplemented with 0.1% Dextran–Texas Red. Cells were held at −80 mV, and voltage steps from −120 mV to +40 mV were applied in 10-mV increments for 500 ms. Steady-state currents were measured during the final portion of each voltage step.

Imaging astrocytic Ca^{2+} activity in slices

To image Ca^{2+} activity in NAcSh astrocytes, GCaMP6f was expressed in astrocytes by crossing *Aldh1l1*-Cre/ERT2 transgenic mice with ROSA26-Lck-GCaMP6f-flox-GFP reporter mice (The Jackson Laboratory, stock nos. 029655 and 029626). Offspring of both sexes, aged 8–16 weeks, received five daily intraperitoneal injections of tamoxifen (100 mg/kg, dissolved in corn oil; VWR, #9001-30-7) to induce astrocyte-specific GCaMP6f expression.

Three weeks after the last tamoxifen injection, coronal slices (200-μm thick) containing the NAcSh were prepared and incubated as described above. All recordings were performed in the continuous presence of TTX (1 μM). GCaMP6f fluorescence signals were captured using a Hamamatsu ORCA-ER C4742 CCI camera mounted on an Olympus BX51W1 microscope through the 488-nm filter. The camera was set with a fixed exposure time of 500 ms and a frame speed of 2 fps. The temperature of the imaging chamber was set at ~31°C. The imaging was confined to the medial ventral portion of the NAcSh through a 40× water immersion objective lens. The sampling area of the slice was 36,000 μm^2 (1344 × 1024 pixels). To generate heatmaps and time courses of astrocytic Ca^{2+} activity (z-score), baseline GCaMP6f fluorescence was recorded for 2 min, followed by perfusion with SKF81297 (1 μM) for an additional 6 min. In some experiments, GCaMP6f fluorescence was measured repeatedly, with each recording lasting 3 min and separated by a 3-min interval.

For experiments involving astrocytic shD1R expression and the corresponding controls, double-transgenic mice (*Aldh1l1*-Cre/ERT2 x ROSA26-Lck-GCaMP6f-flox-GFP) received intra-NAcSh injections of either AAV2/5-GfaABC1D-shD1R-tdTomato or AAV2/5-GfaABC1D-tdTomato. One week after viral injection, intraperitoneal tamoxifen administration was initiated, and Ca^{2+} imaging experiments were performed three weeks after the completion of tamoxifen treatment. To select the areas of interest (AOI) originating from astrocytes infected by either shD1R AAV or control AAV, extracted AOIs were overlaid with the tdTomato fluorescence images, and those overlapping with tdTomato signals were included for further analysis.

Fluorescence signals were pre-processed in ImageJ using the rolling ball algorithm to remove uneven background illumination across frames. Each video was then subjected to motion correction (NoRMCorre algorithm), source extraction and deconvolution in Python using the

Calcium Imaging Analysis (CaImAn) software package, followed by high-pass filtering. A modified version of the constrained nonnegative matrix factorization framework (CNMF-E), specialized for de-mixing and de-noising one-photon imaging data, was used to extract fluorescent signals. The spatial-temporal features (including shapes, locations, and peaks of Ca^{2+} transients) extracted by CNMF-E were subsequently used to identify and classify fluorescent events.

To isolate astrocytic activities and minimize noise and neuropil contamination, only fluorescent events with a signal-to-noise ratio (SNR) greater than 2 were retained for further analysis. A customized Python script was developed to analyze Ca^{2+} transients. Ca^{2+} transients were included in the analysis if their peak amplitudes were at least twofold higher than the baseline standard deviation and separated by at least 1000 ms. Ca^{2+} transients were plotted based on the signals extracted by CNMF-E. Each AOI, defined as a region with fluorescent events exceeding an SNR of 2, was considered a separate astrocyte domain. Event locations were counted as the number of such AOIs, events per AOI as the mean number of Ca^{2+} transients per AOI in the field of view, and events per slice as the total number of transients across the recording period. The percentage change in AOI size was the total net change in fluorescence over baseline multiplied by transient duration, normalized to mean baseline fluorescence intensity.

Immunohistochemistry and confocal microscopy

Mice were transcardially perfused with 0.1 M sodium phosphate buffer, followed by 4% paraformaldehyde (PFA) in 0.1 M phosphate buffer. Brains were removed and postfixed in 4% PFA overnight at 4°C. Whole brains were then stored in 30% sucrose in phosphate buffer with 0.1% sodium azide at 4°C until sectioning. Coronal sections (30-μm thick) containing the NAc

were cut on a microtome (Leica) and collected in 4°C PBS. Sections were incubated overnight at 4°C with primary antibodies against NeuN (mouse, 1:500; Cell Signaling Technology, #94403), GFAP (rabbit, 1:500; Agilent/Dako, #Z0334, or chicken, 1:500; Aves Labs, #GFAP; RRID:AB_2313547), SOX9 (rabbit monoclonal, 1:200; Invitrogen, #MA557739) or IBA1 (rabbit polyclonal, 1:500; Invitrogen, #PA5-143610), as appropriate for each experiment. Sections were then washed three times in PBS (5 min each) and incubated for 2 h at room temperature with Alexa Fluor 488– or 594–conjugated secondary antibodies (1:300; Invitrogen, Thermo Fisher Scientific): donkey anti-mouse IgG (#A-21203) for NeuN, donkey anti-rabbit IgG (#A21206 or #A21207) for GFAP, SOX9 and IBA1, and goat anti-chicken IgY (#A11039) for chicken anti-GFAP. In the displayed images, the Alexa Fluor 594 channel was rendered in magenta. Sections were washed again 3 × 5 min in PBS before they were mounted in ProLong Gold Antifade with DAPI (Molecular Probes).

Sections were imaged using a Leica TCS SP5 confocal microscope controlled by Leica Application Suite software. Images were acquired with a 5× air objective and 40× or 60× oil-immersion objectives. Whole-slice images were obtained using automated tile scanning followed by image stitching.

RNAscope in situ hybridization and immunofluorescence

RNAscope in situ hybridization was performed on 15-µm-thick fixed-frozen coronal brain sections containing the NAcSh using the RNAscope Multiplex Fluorescent Reagent Kit v2 (Advanced Cell Diagnostics, #323100), following the manufacturer's instructions with a protease-free pretreatment workflow. *Drd1* mRNA was detected using a mouse *Drd1*-specific probe

assigned to the C1 channel (Advanced Cell Diagnostics, #461901), with signal detection using Opal 620 (1:1000; Akoya Biosciences, #FP1495001KT).

Following completion of RNAscope detection, sections were immunostained for SOX9 as described above, using Alexa Fluor 488–conjugated donkey anti-rabbit IgG (1:300; Invitrogen, Thermo Fisher Scientific, #A21206) as the secondary antibody.

Drd1 mRNA puncta were manually counted within SOX9-positive nuclei. SOX9-positive nuclei containing at least one *Drd1* punctum were considered *Drd1*-positive, and the proportion of *Drd1*-positive SOX9-positive nuclei and the number of *Drd1* puncta per SOX9-positive nucleus were quantified.

Astrocyte morphological analysis

Astrocyte surface area was quantified from confocal images using Fiji (ImageJ, NIH). Z-stack images of tdTomato-labeled astrocytes in the NAcSh were acquired using identical imaging settings across all experimental groups. Maximum intensity projections were generated for analysis. Individual astrocytes with clearly identifiable somas and non-overlapping processes were manually selected. Cell boundaries were traced using the freehand selection tool based on tdTomato fluorescence, and the enclosed area was measured using the “Measure” function in Fiji. All measurements were performed by an experimenter blind to each mouse’s treatments.

Sholl analysis was performed to quantify the morphological complexity of astrocytes. Individual astrocytes were reconstructed from confocal z-stack images using ImageJ/Fiji. Images were first background-subtracted and thresholded, and individual astrocytes were manually isolated to

exclude overlapping processes from neighboring cells. Binary images were then generated and skeletonized prior to analysis. Sholl analysis was conducted using the Sholl Analysis plugin in ImageJ/Fiji. Concentric circles were drawn at 1-μm intervals centered on the soma of each astrocyte, and the number of process intersections at each radial distance from the soma was quantified. Sholl intersection profiles were averaged across cells within each experimental group and plotted as a function of distance from the soma.

Drugs and reagents

Cocaine hydrochloride (HCl), provided by the NIDA Drug Supply Program, was dissolved in 0.9% NaCl saline. Ketamine and xylazine, purchased from a Drug Enforcement Administration–designated vendor at the University of Pittsburgh, were mixed for anesthesia. All other chemicals were purchased from Sigma-Aldrich, Tocris, J.T. Baker, Fluka, or Alomone Labs.

Statistics

All results are presented as mean ± SEM. Data collection was randomized. Sample sizes were determined based on previous studies using similar experimental approaches (15, 16). All data were analyzed offline, with investigators blinded to experimental conditions during analysis.

A total of 305 mice were used in this study, of which 95 were excluded from the final data analysis and interpretation for the following reasons: (1) 37 mice were excluded due to post-surgical health issues (for example, a >20% reduction in body weight); (2) 41 mice were excluded due to catheter failure or failure to meet self-administration criteria; and (3) 17 mice were

excluded due to off-target stereotaxic injections or poor virus expression. Repeated experiments within the same experimental group were pooled for statistical analysis.

For electrophysiological experiments, sample sizes are presented as n/m, where n represents the number of cells and m represents the number of mice. For behavioral experiments, sample sizes are presented as n, representing the number of mice. Sample sizes and statistical units for other measurements are specified in the relevant figure legends. Two-group comparisons were made using two-tailed unpaired t tests, with Welch's correction applied when variances were unequal, or two-tailed paired t tests for within-subject comparisons, as specified in the relevant figure legends. Multiple-group comparisons were made using one-way or two-way ANOVA, including repeated-measures designs where appropriate, and significant ANOVA results were followed by Bonferroni-corrected post hoc tests. The Greenhouse–Geisser correction was applied when the assumption of sphericity was violated, and non-integer degrees of freedom in the figure legends reflect this correction. Complete post hoc test results are provided in the Supporting Data Values file. Statistical significance was set at $p < 0.05$ for all analyses. Statistical analyses were performed using GraphPad Prism (v.8); statistical analyses of single-nucleus RNA-sequencing data were performed in R as described above.

Study approval

All animal experiments were performed in accordance with protocols approved by the Institutional Animal Care and Use Committee at the University of Pittsburgh.

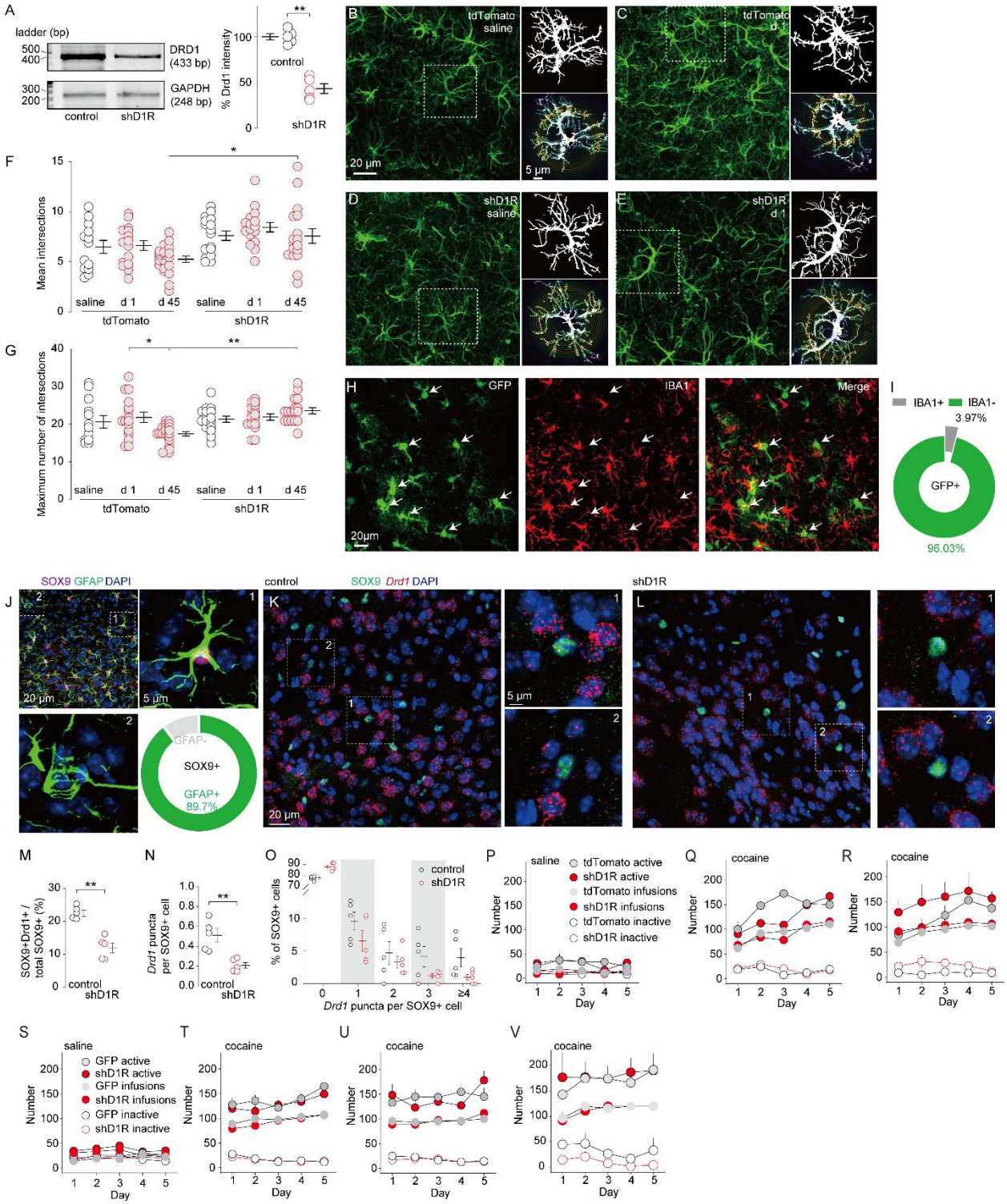
Data availability

Single-nucleus RNA sequencing data are publicly available in the NCBI Gene Expression Omnibus (GEO) under accession number GSE325909. Values for all data points in graphs are reported in the Supporting Data Values file. Custom code used for calcium-imaging data extraction and analysis is publicly available on GitHub (commit ID: ac678c47c9ef0569578cb6b4e7d576315be2db29). The single-nucleus RNA-seq analysis script is publicly available on GitHub (commit ID: 21a4afa689395d5e1f69c17300dc2393c58f82a8).

Supplemental References

1. Wang J, et al. Cocaine Triggers Astrocyte-Mediated Synaptogenesis. *Biol Psychiatry.* 2021;89(4):386-97.
2. Krüger JM, et al. Differential roles of postsynaptic density-93 isoforms in regulating synaptic transmission. *J Neurosci.* 2013;33(39):15504-17.
3. Chen Z, et al. Single-nucleus chromatin accessibility and RNA sequencing reveal impaired brain development in prenatally e-cigarette exposed neonatal rats. *iScience.* 2022;25(8):104686.
4. Hao Y, et al. Dictionary learning for integrative, multimodal and scalable single-cell analysis. *Nat Biotechnol.* 2024;42(2):293-304.
5. Germain PL, et al. Doublet identification in single-cell sequencing data using scDblFinder. *F1000Res.* 2021;10:979.
6. Yu J, et al. Nucleus accumbens feedforward inhibition circuit promotes cocaine self-administration. *Proc Natl Acad Sci U S A.* 2017;114(41):E8750-E9.
7. He Y, et al. Cue- versus reward-encoding basolateral amygdala projections to nucleus accumbens. *Elife.* 2023;12.
8. He Y, et al. Membrane excitability of nucleus accumbens neurons gates the incubation of cocaine craving. *Neuropsychopharmacology.* 2023;48(9):1318-27.
9. Wang YQ, et al. AMPA and NMDA Receptor Trafficking at Cocaine-Generated Synapses. *J Neurosci.* 2021;41(9):1996-2011.
10. Wright WJ, et al. Silent synapses dictate cocaine memory destabilization and reconsolidation. *Nat Neurosci.* 2020;23(1):32-46.
11. Huang YH, et al. In vivo cocaine experience generates silent synapses. *Neuron.* 2009;63(1):40-7.
12. Liao D, et al. Activation of postsynaptically silent synapses during pairing-induced LTP in CA1 region of hippocampal slice. *Nature.* 1995;375(6530):400-4.
13. Suska A, et al. Selective presynaptic enhancement of the prefrontal cortex to nucleus accumbens pathway by cocaine. *Proc Natl Acad Sci U S A.* 2013;110(2):713-8.
14. Ma YY, et al. Bidirectional modulation of incubation of cocaine craving by silent synapse-based remodeling of prefrontal cortex to accumbens projections. *Neuron.* 2014;83(6):1453-67.
15. Neumann PA, et al. Increased excitability of lateral habenula neurons in adolescent rats following cocaine self-administration. *Int J Neuropsychopharmacol.* 2014;18(6).
16. Wang YQ, et al. Neuropathic pain generates silent synapses in thalamic projection to anterior cingulate cortex. *Pain.* 2021;162(5):1322-33.

Supplemental Figure 1.



(**A**) Representative RT-PCR images and summary showing decreased levels of *Drd1* in cultured astrocytes expressing shD1R. Quantification of *Drd1* band intensity expressed as a percentage of the control group (set as 100%). Data are presented as mean ± SEM (Control, 100 ± 3.4, n = 5;

shD1R, 43.2 ± 5.3, n = 5, $t_{6.7} = 9.0$, $p < 0.01$, unpaired Welch's *t* test). Each data point represents an independent culture. **$p < 0.01$.

(**B–E**) Representative GFAP immunostaining of NAcSh slices from tdTomato and shD1R-tdTomato mice at abstinence day 1 following saline or cocaine self-administration. Dashed boxes indicate regions shown at higher magnification. Right panels show reconstructed single astrocytes and the corresponding Sholl analyses. (**F**) Quantification of mean Sholl intersections, calculated as the average number of intersections across all concentric radii for each reconstructed astrocyte at abstinence day 1 and day 45 (tdTomato-saline, 6.5 ± 0.7, n = 13/3; tdTomato-d1, 6.6 ± 0.5, n = 16/3; tdTomato-d45, 5.3 ± 0.3, n = 20/4; shD1R-saline, 7.6 ± 0.5, n = 16/3; shD1R-d1, 8.5 ± 0.5, n = 16/4; shD1R-d45, 7.6 ± 0.7, n = 17/3. $F_{5,92} = 5.0$, $p < 0.01$, one-way ANOVA; $p = 0.02$ tdTomato-d45 vs. shD1R-d45, Bonferroni posttests). (**G**) Quantification of maximum Sholl intersections, defined as the peak number of intersections observed across all radii for each astrocyte at abstinence day 1 and day 45 (tdTomato-saline, 20.7 ± 1.9, n = 13/3; tdTomato-d1, 22.1 ± 1.6, n = 16/3; tdTomato-d45, 16.9 ± 0.7, n = 20/4; shD1R-saline, 21.6 ± 1, n = 16/3; shD1R-d1, 22.3 ± 1, n = 16/4; shD1R-d45, 24.2 ± 1, n = 17/3. $F_{5,92} = 5.0$, $p < 0.01$, one-way ANOVA; $p = 0.02$ tdTomato-d1 vs. tdTomato-d45; $p < 0.01$ tdTomato-d45 vs. shD1R-d45, Bonferroni posttests). Each dot represents one astrocyte. Data are presented as mean ± SEM. *$p < 0.05$, **$p < 0.01$.

(**H**) Example confocal images of the NAc shell from a mouse injected with AAV2/5-GfaABC1D-shD1R-GFP, showing virally expressed GFP (green, left), IBA1 immunofluorescence (red, middle), and the image with green and red channels merged (right). Arrows indicate the locations of the same GFP^+ cells from the left panel. (**I**) Quantification of GFP/IBA1 co-labeling: 5 out of 115 GFP^+ cells were $IBA1^+$, corresponding to 3.97 ± 2.03% of GFP^+ cells across sampled fields.

Conversely, 5 out of 358 $IBA1^+$ cells were GFP^+, corresponding to 1.43 ± 0.78% of $IBA1^+$ cells. Data were obtained in 9 imaging fields from 3 mice.

(**J**) Example image showing SOX9 (magenta), GFAP (green) and DAPI (blue) signals in NAcSh cells. High magnification of the boxed region 1 showing an $SOX9^+$ and $GFAP^+$ cell with the SOX9 immunoreactivity confined to the $DAPI^+$ nucleus. High magnification of the boxed region 2 showing a $GFAP^+$ cell lacking SOX9 signal. Summary of SOX9-GFAP co-localization: 89.7% of $SOX9^+$ cells were $GFAP^+$ (n = 301 cells from 3 mice), validating SOX9 as an astrocytic nuclear marker in the NAcSh. (**K and L**) Example RNAscope images of *Drd1* mRNA (red) combined with immunostaining of SOX9 (green) and DAPI nuclear counterstaining (blue) from control (**K**) and shD1R (**L**) mice. (**M**) Summary showing the % of $SOX9^+$ cells containing *Drd1* mRNA puncta (in %: control, 22.7 ± 0.8, n = 5; shD1R, 12.0 ± 1.5, n = 5, $t_{6.3} = 6.2$, $p < 0.01$, unpaired Welch's *t* test). (**N**) Summary showing the number of *Drd1* mRNA puncta per $SOX9^+$ cell (control, 0.51 ± 0.07, n = 5; shD1R, 0.21 ± 0.03, n = 5, $t_{5.4} = 4.1$, $p < 0.01$, unpaired Welch's *t* test). Each circle represents one mouse. (**O**) Distribution of *Drd1* mRNA puncta per $SOX9^+$ cell, expressed as the % of all $SOX9^+$ cells in each bin (n = 5 mice per group; 437 and 395 $SOX9^+$ cells for control and shD1R, respectively). Scale bars: 20 μm (low-magnification images) and 5 μm (high-magnification images). *$p < 0.05$; **$p < 0.01$.

(**P–R**) Summarized results of self-administration training of the mice used for morphological studies (Figure 4), including mice with saline self-administration and one day of abstinence (tdTomato n = 3, shD1R n = 4; **P**), mice with cocaine self-administration and one day of abstinence (tdTomato n = 4, shD1R n = 4; **Q**) and mice with cocaine self-administration and 45 days of abstinence (tdTomato n = 4, shD1R n = 3; **R**). (**S–U**) Summarized results of self-administration training of the mice used for physiological studies (Figure 5), including mice with saline self-administration (GFP n = 14, shD1R n = 15; **S**), mice with cocaine self-administration

and one day of abstinence (GFP n = 13, shD1R n = 14; **T**) and mice with cocaine self-administration and 45 days of abstinence (GFP n = 16, shD1R n = 17; **U**). (**V**) Summarized results of self-administration training of the mice used for behavioral studies (Figure 6) (GFP n = 8, shD1R n = 7); lever-press data from this cohort are also shown in Figure 6B.

Supplemental Table 1. Related to Figure 1. Extracellular matrix, adhesion, and cytoskeletal genes differentially expressed in nucleus accumbens astrocytes after cocaine self-administration and abstinence.

Gene	avg log_2FC	pct.1	pct.2	adj. *p*	Interpretation
Extracellular matrix and matrix remodeling					
Mmp16	−0.974	0.147	0.236	4.64×10^{-8}	Membrane-type MMP
Sparc	+0.931	0.233	0.125	1.70×10^{-9}	Astrocyte-secreted matricellular protein (Figure 1E)
Timp2	+0.792	0.240	0.132	2.75×10^{-9}	MMP regulator; endogenous metalloproteinase inhibitor
Adamts6	−0.776	0.156	0.237	6.04×10^{-4}	ADAMTS metalloproteinase
Dock11	−0.604	0.180	0.242	4.49×10^{-2}	Cdc42 guanine-nucleotide exchange factor (Figure 1E)
Igsf21	−0.585	0.158	0.232	4.01×10^{-2}	Immunoglobulin superfamily adhesion molecule (Figure 1E)
Adam23	−0.497	0.533	0.648	8.93×10^{-12}	ADAM-family adhesion-associated protein
Tspan7	−0.461	0.903	0.934	1.65×10^{-32}	Tetraspanin-7; process stabilization (Figure 1E)
Lama2	−0.382	0.761	0.822	5.15×10^{-13}	Laminin α2, integrin ligand (Figure 1E)
Adhesion-associated signaling					
Ptk2b	+0.749	0.217	0.126	9.95×10^{-6}	PYK2, a CNS-enriched FAK-family kinase; Ptk2 itself was not identified as a DEG
Tln2	+0.585	0.310	0.218	5.20×10^{-4}	Talin-2; links integrins to the actin cytoskeleton
Vcl	−0.396	0.569	0.630	3.54×10^{-7}	Vinculin, focal-adhesion adaptor
Actin cytoskeletal regulation					
Cfl1	+0.817	0.305	0.176	2.38×10^{-11}	Cofilin-1; actin depolymerization (Figure 1E)
Actb	+0.795	0.831	0.650	2.98×10^{-49}	β-actin (Figure 1E)
Tuba1a	+0.794	0.354	0.212	5.71×10^{-13}	Tubulin α1a (Figure 1E)
Actg1	+0.697	0.626	0.438	1.03×10^{-22}	γ-actin (Figure 1E)
Rhou	+0.624	0.265	0.189	1.47×10^{-2}	Rho-family GTPase; actin cytoskeletal remodeling
Pfn2	+0.617	0.315	0.218	1.45×10^{-4}	Profilin-2; actin polymerization
Wasf1	+0.580	0.321	0.210	1.59×10^{-6}	WAVE1; Arp2/3 activator (Figure 1E)
Cdc42	+0.544	0.393	0.276	1.42×10^{-6}	Filopodial process formation
Arpc2	+0.423	0.290	0.208	2.27×10^{-2}	Arp2/3 complex subunit

Genes shown are those identified as differentially expressed in the astrocyte nuclei cluster by comparing cocaine self-administration and abstinence with control. pct.1 and pct.2 denote the proportion of astrocyte nuclei in which each transcript was detected in the cocaine and control groups, respectively. Genes annotated Figure 1D or Figure 1E are those already presented in the main figure. Thrombospondin family genes (Thbs1, Thbs2), Cacna2d1 (α2δ-1), and integrin subunit genes were not identified as differentially expressed and therefore are not included in the table.

Supplemental Table 2. Related to Figure 5. Analysis of sex as a factor in the percentage of silent synapses.

Measure	Sex	Virus × Sex
Abstinence day 1 (Figure 5E)		
% of silent synapses	$F(1,15) = 0.09$, $p = 0.76$	$F(1,15) = 0.02$, $p = 0.90$
Abstinence day 45, vehicle (Figure 5J)		
% of silent synapses	$F(1,22) = 0.11$, $p = 0.74$	$F(1,22) = 0.08$, $p = 0.77$
Abstinence day 45, Naspm (Figure 5J)		
% of silent synapses	$F(1,13) = 0.52$, $p = 0.48$	$F(1,13) = 0.13$, $p = 0.72$

Data were analyzed by two-way ANOVA with virus and sex as between-subject factors, with each value representing the mean of all cells recorded from one mouse. The vehicle and Naspm conditions were analyzed separately. Animal numbers: cocaine-GFP, 5 male and 4 female; cocaine-shD1R, 5 male and 5 female; cocaine-GFP-vehicle, 6 male and 5 female; cocaine-shD1R-vehicle, 9 male and 6 female; cocaine-GFP-Naspm, 4 male and 4 female; cocaine-shD1R-Naspm, 5 male and 4 female. No sex-dependent effects were detected.

Supplemental Table 3. Related to Figure 6. Analysis of sex as a factor in behavioral outcome measures.

Measure	Sex	Virus × Sex
Cocaine self-administration (5-day average) (Figure 6B)		
Active lever presses	$F(1,11) = 0.67$, $p = 0.43$	$F(1,11) = 0.01$, $p = 0.92$
Inactive lever presses	$F(1,11) = 3.95$, $p = 0.07$	$F(1,11) = 0.26$, $p = 0.62$
Extinction day 10 (Figure 6C)		
Active lever presses	$F(1,10) = 0.42$, $p = 0.53$	$F(1,10) = 0.21$, $p = 0.65$
Inactive lever presses	$F(1,10) = 1.23$, $p = 0.29$	$F(1,10) = 1.83$, $p = 0.21$
Cue-induced reinstatement (3-day average) (Figure 6D)		
Active lever presses	$F(1,10) = 0.15$, $p = 0.71$	$F(1,10) = 0.0002$, $p = 0.99$

Measure	Sex	Virus × Sex
Inactive lever presses	$F(1,10) = 0.42$, $p = 0.53$	$F(1,10) = 1.50$, $p = 0.25$

Data were analyzed by two-way ANOVA with virus and sex as between-subject factors. Animal numbers: GFP, 4 male and 4 female throughout; shD1R, 4 male and 3 female for self-administration and 3 male and 3 female for extinction and reinstatement (one male mouse did not complete the procedure). The effect of sex and the virus × sex interaction are reported here, as these are the terms relevant to whether the reported effects differ between sexes. No sex-dependent effects were detected.

Supplemental Table 4. Descriptive statistics and statistical tests for the main and supplemental figures.

Values are mean ± SEM. For F tests, degrees of freedom are shown as numerator, denominator; for t tests, a single value is shown.

Figure panel	Outcome	Sample size	Mean ± SEM	Statistical test	Statistic	*p*
Figure 2H	Current–voltage relationship, group effect	control, n = 11/6 shD1R, n = 12/6	Units: pA control: 1237 ± 383.6 shD1R: 1615 ± 503.0	Two-way RM ANOVA, GG corrected	$F(1, 21) = 1.0$	= 0.32
Figure 2H	Current–voltage relationship, voltage × group	As above (Figure 2H)	As above (Figure 2H)	Two-way RM ANOVA, GG corrected	$F(1, 21.1) = 1.1$	= 0.31
Figure 2I	Whole-cell capacitance	GFP, n = 11/6 shD1R, n = 11/5	Units: pF GFP: 21.17 ± 4.4 shD1R: 23.2 ± 5.0	Unpaired Welch's t test	$t(19.7) = 0.3$	= 0.76
Figure 2I	Membrane resistance	GFP, n = 10/6 shD1R, n = 12/5	Units: MΩ GFP: 33.6 ± 4.5 shD1R: 30.1 ± 4.6	Unpaired Welch's t test	$t(19.9) = 0.5$	= 0.59
Figure 2I	Resting membrane potential	GFP, n = 12/6 shD1R, n = 11/5	Units: mV GFP: −81.1 ± 0.9 shD1R: −81.7 ± 1.2	Unpaired Welch's t test	$t(19.3) = 0.4$	= 0.68
Figure 2J	Paired-pulse ratio	control, n = 17/6 shD1R, n = 13/6	control: 1.0 ± 0.1 shD1R: 1.0 ± 0.0	Unpaired Welch's t test	$t(27.2) = 0.5$	= 0.64
Figure 3F	Number of active AOIs	n = 10 slices from 4 mice	before: 114.6 ± 16.8 SKF: 147.9 ± 24.7	Paired two-tailed t test	$t(9) = 3.5$	< 0.01
Figure 3F	Ca2+ events per AOI in 3 min	n = 10 slices from 4 mice	before: 2.5 ± 0.1 SKF: 2.9 ± 0.2	Paired two-tailed t test	$t(9) = 2.4$	= 0.04
Figure 3F	Total Ca2+ events per slice in 3 min	n = 10 slices from 4 mice	before: 283.7 ± 46.2 SKF: 441.8 ± 91.0	Paired two-tailed t test	$t(9) = 3.0$	= 0.02
Figure 3F	AOI size relative to baseline	n = 10 slices from 4 mice	Units: % SKF: 141.4 ± 12.8	Paired two-tailed t test	$t(9) = 3.3$	= 0.01
Figure 3I	Ca2+ events, tdTomato control	44 AOIs 10 slices/4–5 mice per group[1]	before: 2.0 ± 0.2 SKF: 2.8 ± 0.3	Paired two-tailed t test	$t(43) = 2.2$	= 0.03
Figure 3I	AOI size, tdTomato control	43 AOIs 10 slices/4–5 mice per group[1]	Units: % SKF: 177.9 ± 19.0	Paired two-tailed t test	$t(42) = 4.1$	< 0.01
Figure 3I	Ca2+ events, shD1R	51 AOIs 10 slices/4–5 mice per group[1]	before: 2.2 ± 0.2 SKF: 2.0 ± 0.2	Paired two-tailed t test	$t(50) = 0.6$	= 0.56
Figure 3I	AOI size, shD1R	48 AOIs 10 slices/4–5 mice per group[1]	Units: % SKF: 116.1 ± 14.1	Paired two-tailed t test	$t(47) = 1.1$	= 0.26

Figure panel	Outcome	Sample size	Mean ± SEM	Statistical test	Statistic	*p*
Figure 4B	Astrocyte surface area, group effect	tdTomato saline, n = 15/3 tdTomato d1, 16/4 tdTomato d45, 17/4 shD1R saline, 16/4 shD1R d1, 16/4 shD1R d45, 15/3	Units: 10^3 µm² tdTomato saline: 1.1 ± 0.1 tdTomato d1: 0.6 ± 0.1 tdTomato d45: 0.5 ± 0.1 shD1R saline: 0.9 ± 0.1 shD1R d1: 1.1 ± 0.1 shD1R d45: 1.0 ± 0.1	One-way ANOVA	$F(5, 89) = 6.9$	< 0.01
Figure 4B	tdTomato saline vs. tdTomato d1	As above (Figure 4B)	As above (Figure 4B)	Bonferroni posttest	NR	= 0.02
Figure 4B	tdTomato saline vs. tdTomato d45	As above (Figure 4B)	As above (Figure 4B)	Bonferroni posttest	NR	< 0.01
Figure 4B	tdTomato d1 vs. shD1R d1	As above (Figure 4B)	As above (Figure 4B)	Bonferroni posttest	NR	= 0.04
Figure 4B	tdTomato d45 vs. shD1R d45	As above (Figure 4B)	As above (Figure 4B)	Bonferroni posttest	NR	< 0.01
Figure 4D	Sholl intersections, group effect	tdTomato saline, n = 13/3 tdTomato d1, 16/3 tdTomato d45, 21/4 shD1R saline, 16/3 shD1R d1, 17/4 shD1R d45, 17/3	tdTomato saline: 7.8 ± 1.1 tdTomato d1: 7.2 ± 1.2 tdTomato d45: 5.6 ± 0.9 shD1R saline: 8.4 ± 1.1 shD1R d1: 9.0 ± 1.1 shD1R d45: 9.1 ± 1.2	Ordinary two-way ANOVA	$F(5, 3384) = 73.6$	< 0.01
Figure 4D	Sholl intersections, group × distance	As above (Figure 4D)	As above (Figure 4D)	Ordinary two-way ANOVA	$F(175, 3384) = 2.3$	< 0.01
Figure 4D	tdTomato saline vs. tdTomato d45	As above (Figure 4D)	As above (Figure 4D)	Bonferroni posttest	NR	< 0.01
Figure 4D	tdTomato d1 vs. tdTomato d45	As above (Figure 4D)	As above (Figure 4D)	Bonferroni posttest	NR	< 0.01
Figure 4D	tdTomato d45 vs. shD1R d45	As above (Figure 4D)	As above (Figure 4D)	Bonferroni posttest	NR	< 0.01
Figure 5E	Silent synapses on abstinence day 1, group effect	saline-GFP, n = 10/5 saline-shD1R, 12/5 cocaine-GFP, 16/9 cocaine-shD1R, 14/10	Units: % saline-GFP: 8.6 ± 2.5 saline-shD1R: 9.0 ± 3.3 cocaine-GFP: 38.6 ± 3.1 cocaine-shD1R: 23.9 ± 4.8	One-way ANOVA	$F(3, 48) = 15.8$	< 0.01
Figure 5E	saline-GFP vs. cocaine-GFP	As above (Figure 5E)	As above (Figure 5E)	Bonferroni posttest	NR	< 0.01
Figure 5E	saline-shD1R vs. cocaine-shD1R	As above (Figure 5E)	As above (Figure 5E)	Bonferroni posttest	NR	= 0.04
Figure 5E	cocaine-GFP vs. cocaine-shD1R	As above (Figure 5E)	As above (Figure 5E)	Bonferroni posttest	NR	= 0.02
Figure 5F	NMDAR EPSC amplitude after Ro256981, saline	GFP, n = 9/5 shD1R, n = 8/6	Units: % of baseline GFP: 94.1 ± 1.2 shD1R: 100.5 ± 1.4	Two-way RM ANOVA, group effect	$F(1, 15) = 0.6$	= 0.46
Figure 5G	NMDAR EPSC amplitude after Ro256981, cocaine	GFP, n = 9/4 shD1R, n = 9/4	Units: % of baseline GFP: 77.7 ± 1.3 shD1R: 92.7 ± 2.0	Two-way RM ANOVA, group effect	$F(1, 16) = 5.6$	= 0.03

Figure panel	Outcome	Sample size	Mean ± SEM	Statistical test	Statistic	*p*
Figure 5J	Silent synapses on abstinence day 45, group effect	saline-GFP, n = 10/4 saline-shD1R, 12/4 cocaine-GFP-vehicle, 14/11 cocaine-GFP-Naspm, 11/8 cocaine-shD1R-vehicle, 20/15 cocaine-shD1R-Naspm, 11/9	Units: % saline-GFP: 8.4 ± 2.3 saline-shD1R: 9.7 ± 3.0 cocaine-GFP-vehicle: 5.1 ± 1.7 cocaine-GFP-Naspm: 41.1 ± 4.4 cocaine-shD1R-vehicle: 14.4 ± 2.4 cocaine-shD1R-Naspm: 24.8 ± 5.8	One-way ANOVA	$F(5, 72) = 14.8$	< 0.01
Figure 5J	saline-GFP vs. cocaine-GFP-Naspm	As above (Figure 5J)	As above (Figure 5J)	Bonferroni posttest	NR	< 0.01
Figure 5J	cocaine-GFP-vehicle vs. cocaine-GFP-Naspm	As above (Figure 5J)	As above (Figure 5J)	Bonferroni posttest	NR	< 0.01
Figure 5J	cocaine-GFP-Naspm vs. cocaine-shD1R-Naspm	As above (Figure 5J)	As above (Figure 5J)	Bonferroni posttest	NR	= 0.03
Figure 5J	saline-shD1R vs. cocaine-shD1R-Naspm	As above (Figure 5J)	As above (Figure 5J)	Bonferroni posttest	NR	= 0.049
Figure 6B	Acquisition, active lever presses (5-day average)	control, n = 8 shD1R, n = 7	control: 170.3 ± 19.3 shD1R: 181.5 ± 27.7	Two-way RM ANOVA, GG corrected, time × group	$F(2.2, 29) = 0.4$	= 0.68
Figure 6B	Acquisition, inactive lever presses (5-day average)	control, n = 8 shD1R, n = 7	control: 33.8 ± 9.9 shD1R: 10.2 ± 2.7	Two-way RM ANOVA, GG corrected, time × group	$F(1.9, 24.7) = 0.2$	= 0.84
Figure 6C	Extinction day 10, active lever presses	GFP, n = 8 shD1R-GFP, n = 6	GFP: 86.1 ± 26.0 shD1R-GFP: 21.5 ± 5.6	Two-tailed Welch's t test	$t(7.6) = 2.4$	= 0.04
Figure 6C	Extinction day 10, inactive lever presses	GFP, n = 8 shD1R-GFP, n = 6	GFP: 27.9 ± 11.4 shD1R-GFP: 11.2 ± 7.8	Two-tailed Welch's t test	$t(11.5) = 1.2$	= 0.25
Figure 6D	Reinstatement, active lever presses (3-day average)	GFP, n = 8 shD1R, n = 6	GFP: 157.9 ± 28.5 shD1R: 69.7 ± 19.2	Two-way RM ANOVA, group effect	$F(1, 12) = 5.7$	= 0.04
Figure 6D	Reinstatement, inactive lever presses (3-day average)	GFP, n = 8 shD1R, n = 6	GFP: 16.9 ± 2.5 shD1R: 13.2 ± 7.7	Two-way RM ANOVA, group effect	$F(1, 12) = 0.3$	= 0.6
Suppl. Figure 1A	*Drd1* expression relative to control	control, n = 5 shD1R, n = 5	Units: % control: 100 ± 3.4 shD1R: 43.2 ± 5.3	Unpaired Welch's t test	$t(6.7) = 9.0$	< 0.01
Suppl. Figure 1F	Mean Sholl intersections, group effect	tdTomato-saline, n = 13/3 tdTomato-d1, 16/3 tdTomato-d45, 20/4 shD1R-saline, 16/3 shD1R-d1, 16/4 shD1R-d45, 17/3	tdTomato-saline: 6.5 ± 0.7 tdTomato-d1: 6.6 ± 0.5 tdTomato-d45: 5.3 ± 0.3 shD1R-saline: 7.6 ± 0.5 shD1R-d1: 8.5 ± 0.5 shD1R-d45: 7.6 ± 0.7	One-way ANOVA	$F(5, 92) = 5.0$	< 0.01
Suppl. Figure 1F	tdTomato-d45 vs. shD1R-d45	As above (Suppl. Figure 1F)	As above (Suppl. Figure 1F)	Bonferroni posttest	NR	= 0.02

Figure panel	Outcome	Sample size	Mean ± SEM	Statistical test	Statistic	*p*
Suppl. Figure 1G	Maximum Sholl intersections, group effect	tdTomato-saline, n = 13/3 tdTomato-d1, 16/3 tdTomato-d45, 20/4 shD1R-saline, 16/3 shD1R-d1, 16/4 shD1R-d45, 17/3	tdTomato-saline: 20.7 ± 1.9 tdTomato-d1: 22.1 ± 1.6 tdTomato-d45: 16.9 ± 0.7 shD1R-saline: 21.6 ± 1 shD1R-d1: 22.3 ± 1 shD1R-d45: 24.2 ± 1	One-way ANOVA	$F(5, 92) = 5.0$	< 0.01
Suppl. Figure 1G	tdTomato-d1 vs. tdTomato-d45	As above (Suppl. Figure 1G)	As above (Suppl. Figure 1G)	Bonferroni posttest	NR	= 0.02
Suppl. Figure 1G	tdTomato-d45 vs. shD1R-d45	As above (Suppl. Figure 1G)	As above (Suppl. Figure 1G)	Bonferroni posttest	NR	< 0.01
Suppl. Figure 1I	GFP/IBA1 colabeling	9 imaging fields from 3 mice	Units: % GFP^+ cells that were $IBA1^+$: 3.97 ± 2.03 $IBA1^+$ cells that were GFP^+: 1.43 ± 0.78	NR	NR	NR
Suppl. Figure 1M	$SOX9^+$ cells containing *Drd1* puncta	control, n = 5 shD1R, n = 5	Units: % control: 22.7 ± 0.8 shD1R: 12.0 ± 1.5	Unpaired Welch's t test	$t(6.3) = 6.2$	< 0.01
Suppl. Figure 1N	*Drd1* puncta per $SOX9^+$ cell	control, n = 5 shD1R, n = 5	control: 0.51 ± 0.07 shD1R: 0.21 ± 0.03	Unpaired Welch's t test	$t(5.4) = 4.1$	< 0.01

Notes

1. Slash-separated sample sizes are cells or astrocytes/mice for the electrophysiological and morphological measurements. For Supplemental Figure 1A, n denotes independent cultures; for Supplemental Figure 1, M and N, n denotes mice; for Figure 6, n denotes mice.
2. Bonferroni post hoc comparisons follow the omnibus test of the same panel; "As above" refers to the sample sizes and group values of that omnibus row. The significance symbols used in the figures (*, $p < 0.05$; **, $p < 0.01$) are defined in the figure legends.
3. Figure 1 panels do not contribute entries; the differential-expression statistics for the single-nucleus RNA-sequencing data are described in Methods and reported in the Supporting Data Values file.
4. NR, not reported; SKF, SKF81297; AOI, area of interest; GG, Greenhouse–Geisser; RM, repeated measures; d1 and d45, abstinence days 1 and 45.